Scattering Depolarization Characteristics of 1064 nm Nanosecond Pulsed Circularly polarized laser in Near Ground Aerosol Environments

Hang Yin, Xiyu Jin, Leihao Ma, Hui Chai, Zhibo Bai, Changli Li *
School of Physics, Changchun University of Science and Technology, Changchun 130022, China
Corresponding author email :licl@cust.edu.cn

Abstract Polarization detection is often affected by complex weather conditions, leading to deviations in test information. This is due to the influence of scattering media such as water mist particles and gas molecules in the atmosphere on the propagation of polarized light waves. To address this issue, this paper establishes a depolarization model for the multiple scattering propagation of a 1064 nm nanosecond pulsed circularly polarized laser(NPCPL) in an aerosol environment based on Mie scattering theory and the Monte Carlo algorithm. The depolarization characteristics of polarized light in four typical near-ground aerosol particles are calculated, and the influence of pulse width, concentration, transmission distance, and particle radius on forward scattering depolarization is analyzed. Based on simulation data, an exponential decay fitting model of polarization degree(DOP) as a function of particle concentration, radius, and transmission distance is further proposed. The fitting determination coefficient R^2 reaches 0.952, indicating that this model can comprehensively reflect the influence mechanism of scattering polarization on atmospheric propagation by parameters such as particle concentration, radius, transmission distance, and refractive index. The results show that the DOP decreases under the influence of pulse width, concentration, transmission distance, and particle radius. This is because scattering occurs due to the interaction between photons and the propagation medium. The scattering direction directly determines the scattering intensity of the perpendicular and parallel components, and this difference in intensity leads to polarization. The research findings of this article can provide a theoretical basis for applications of NPCPL in lidar, laser ranging, and wireless laser communication.

Key words 1064 nm narrow-pulse laser; Mie scattering; Monte Carlo; polarization characteristics

1 Introduction

Compared to conventional visible light and infrared detection methods, the detection technology based on polarized light possesses advantages such as multiple information dimensions, strong fog penetration, and minimal interference from background light. Nanosecond pulse lasers play a key role in cutting-edge fields such as lidar [1][2], laser ranging [3][4][5], and wireless laser communication [6][7][8][9] due to their high peak power and accurate time resolution. In particular, the combination of its time resolution characteristics and polarization detection provides a new technical approach for target identification and parameter inversion in complex scattering media. However, the scattering effect of atmospheric aerosols in near-Earth space will significantly interfere with the transmission characteristics of polarization signals, resulting in distortion of the vibration direction of light and a decrease in DOP, thereby reducing detection accuracy and information reliability. Especially in the low-altitude range [10][11][12], a large number of typical aerosol components such as water mist particles, biological

particles, sea salt particles and mineral dust particles, due to their large dynamic changes in concentration, complex particle size distribution and obvious differences in optical properties, become the main factors of signal polarization degradation. Therefore, in-depth research into the scattering mechanisms of these particles and their impact on polarized light transmission is crucial for improving polarization detection capabilities in complex environments.

Existing research focuses on polarization transmission modeling of single particle types [13][14][15], obtaining the scattering polarization influence law under ideal conditions, which has played a certain role in promoting the development of polarization detection technology. However, the polarization characteristics of lasers in the atmosphere are the result of the combined action of multiple particles. At present, no systematic research on polarization effects in multi-particle scenarios, and thus existing models fail to adequately represent the impact of multi-component aerosols in real-world near-ground environments**.** To address this issue, this paper establishes a multi-parameter scattering coupled polarization model based on the improved Monte Carlo method, and systematically studies the polarization transmission characteristics of lasers with different pulse widths in particles such as water mist, biological particles, sea salt, and mineral dust. The influence of pulse width, particle concentration, transmission distance, and particle radius on depolarization is analyzed. The research results can provide a theoretical basis for anti-interference design of laser communication, laser ranging, and lidar using NPCPL in complex environments, and promote the development of high-reliability near-ground polarization optics technology.

2 Polarization transport simulation model based on Monte Carlo simulation

To investigate the propagation characteristics of pulsed lasers in scattering media, a time-resolved Monte Carlo method was employed to track the trajectory of each photon and record its flight time. A predefined time gate was employed to select valid photons, thereby enabling accurate characterization of the temporal evolution of the pulsed laser in the scattering medium. Furthermore, the temporal characteristics of the pulsed laser were combined with the Mie multiple scattering process to further analyze its polarization characteristics in the time domain.

2.1 Pulse laser emission model

Pulsed lasers typically have a Gaussian time distribution, the mathematical expression is:

$$I(t) = I_0 exp\ (-\frac{(t-t_0)^2}{2\sigma^2}) \tag{1}$$

Where I_0 is the peak pulse intensity, t_0 is the pulse center time, and σ is the standard deviation.

Denote by time $t_{1/2}$ be the time point while the intensity drops to half of its peak value, then equation (1) becomes:

$$I(t_{1/2}) = I_0 exp\ (-\frac{(t_{1/2})^2}{2\sigma^2}) \tag{2}$$

Taking the logarithm of both sides of the equation and simplifying it, we get:

$$t_{1/2} = \sigma\sqrt{2ln2} \tag{3}$$

Therefore, the pulse full width at half maximum (FWHM) t_p is:

$$t_p = 2 * \sigma\sqrt{2ln2} \approx 2.355\sigma \tag{4}$$

The initial emission time t_0 of each photon is generated by random sampling from a Gaussian distribution, and its expression is as follows:

$$t_0 = \sigma * \xi_1 \tag{5}$$

Where ξ_1 is a random variable that follows a normal distribution;

To analyze the propagation process of pulsed laser in a medium, a time window $[T_{min}, T_{max}]$ is set as follows:

$$\begin{cases} T_{min} = \frac{L}{c/n} - 6\sigma \\ T_{max} = \frac{L_{max}}{c/n} + 6\sigma \end{cases} \tag{6}$$

To ensure that nearly all photons within the Gaussian temporal envelope are included, the simulation time window is extended to six standard deviations of the pulse width, allowing for an effective utilization of the pulse energy. Where L is the transmission distance, c is the speed of light, n is the refractive index of the medium, and L_{max} is the maximum transmission path, expressed as:

$$L_{max} = N\frac{1}{K_{ext}} \tag{7}$$

Where N is the maximum number of scatterings, and $1/K_{ext}$ is the mean free path.

When photons propagate through a medium, the time-cumulative effect follows:

$$t_{total} = t_0 + \sum_1^i \frac{nl}{c} \tag{8}$$

Where l is the free path.

The laser beam is discretized into a large number of photons, and they are emitted sequentially according to the emission time, spatial position, and direction information of the photons. The spatial position distribution of the photons at the emission time follows a Gaussian distribution, which can be specifically expressed as [16]:

$$\begin{cases} x = \omega_0 * \xi_1 \\ y = \omega_0 * \xi_1 \\ z = 0 \end{cases} \tag{9}$$

Where ω_0 is the beam waist radius of the laser beam. The direction vector at the moment of photon emission is given by the following formula:

$$\begin{cases} u_x = sin\theta_0 cos\beta_0 \\ u_y = sin\theta_0 sin\beta_0 \\ u_z = cos\theta_0 \end{cases} \tag{10}$$

Where $\theta_0 = \left|\frac{\theta'}{2}\xi_1\right|$ is the zenith angle of the photon emission direction, θ' is the divergence angle of the laser beam; $\beta_0 = 2\pi * \xi$ is the azimuth angle of the photon emission direction, and ξ is a random number uniformly distributed in the interval [0,1].

2.2 Laser transmission model

Based on Monte Carlo and Mie scattering, a transmission model of polarized light in particles is established. The transmission and multiple scattering process of randomly sampled photons in the scattering medium is shown in Figure.1. Assuming photons propagate along the z-axis, the incident light stokes vector S_0 is [1;0;0;1], and the initial normalized energy weight of the photon is $\omega = 1$. After the photon undergoes n scatterings in the scattering medium, the energy weight becomes [17]:

$$w(n) = \frac{Ksca}{Kext} * w(n-1) \tag{11}$$

Where ω is the albedo of the scattering medium, which is expressed as the ratio of the volume scattering coefficient to the volume extinction coefficient of the medium. When the photon energy weight is less than the minimum threshold range $w < 10^{-4}$, the photon is considered terminated.

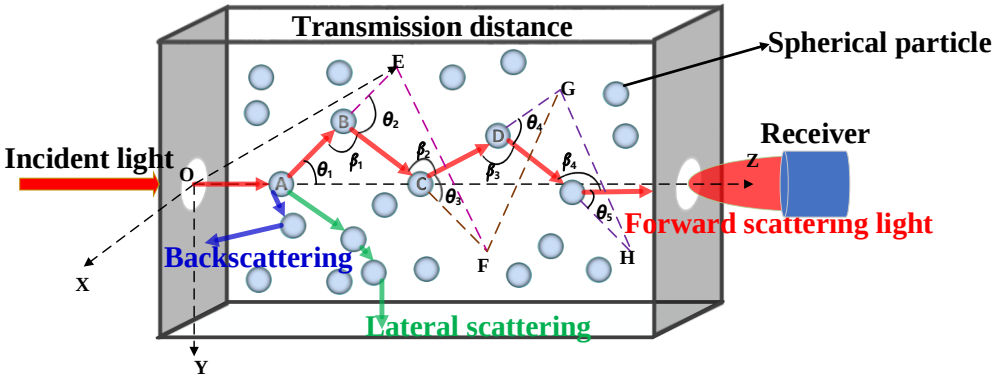

Figure.1. Schematic representation of multiple light scattering in aerosol media

As shown in Figure.1, the propagation path of photons in the medium exhibits a certain degree of randomness, and their scattering behavior can be categorized into three types: forward scattering, side scattering, and back scattering. Considering the application scenarios of NPCPL, the depolarization characteristics of forward scattering are examined in detail. Let the initial reference plane be AOE. As the photon undergoes multiple scatterings, it is sequentially updated to successive reference planes such as BEF, CFG, and DGH. The angle between the new direction of the scattered photon and its original incident direction is called the scattering angle, denoted as θ_1,θ_2,θ_3,θ_4,and θ_5.The rotation angle of the scattering plane relative to the reference plane is called the azimuth angle, denoted as β_1,β_2,β_3,β_4, andβ_5. A schematic diagram of a single scattering plane is shown in Figure. 2.

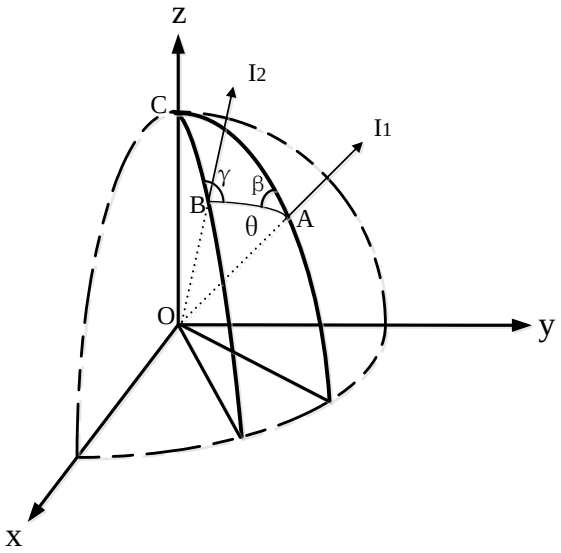

Figure. 2. Schematic of single scattering geometry

As shown in Figure. 2, the photon propagates along the OA direction with an intensity of I_1. After scattering, its propagation direction changes to OB, corresponding to a scattered light intensity of I_2. The angle θ between the incident direction OA and the scattering direction OB is the scattering angle. Because the photon's propagation direction changes after passing through the scattering medium, its vibration plane perpendicular to the propagation direction rotates, thus producing polarization. β and γ represent the angles of rotation between the planes COA and COB and the scattering plane OBA, respectively, before and after scattering. The core steps of the Monte Carlo numerical method are shown in Figure.3, including photon initialization, free path sampling, selection of the scattering direction, photon extinction, and statistical results.

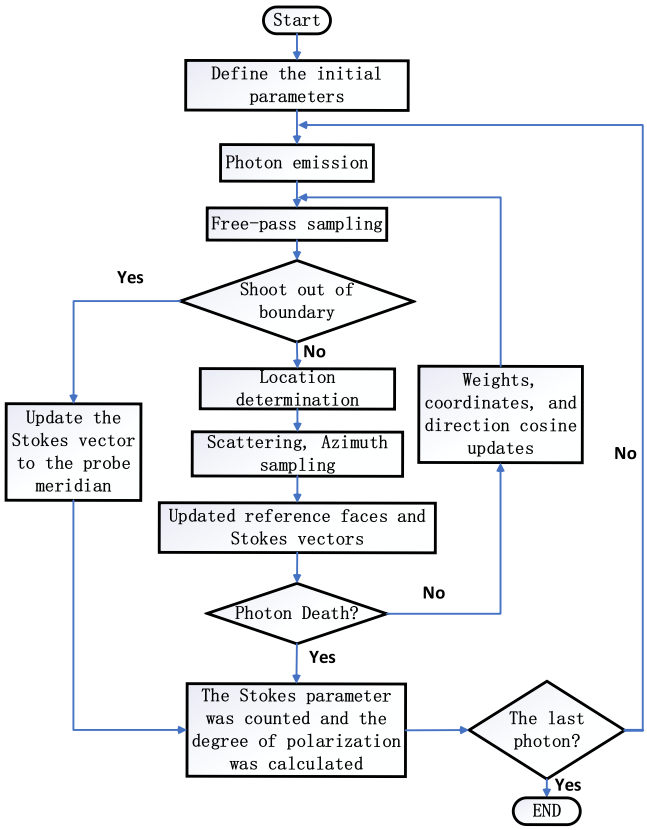

Figure.3. Flowchart of the Monte Carlo simulation procedure

2.2.1 Scattering angle and azimuth angle sampling

When the detector is located in the forward scattering region, according to the rejection sampling method, the scattering angle θ and the azimuth angle β rotated to the scattering plane can be expressed as [18]:

$$\begin{cases} \theta = \pi \bullet \xi \\ \beta = 2\pi \bullet \xi \end{cases} \tag{12}$$

Where the scattering angle $\theta \in (0,\pi)$, the azimuth angle $\beta \in (0,2\pi)$, and satisfy the probability distribution function:

$$P_\theta = 2\pi \int_0^\theta m_{11}(\theta) \sin\theta \, d\theta = \xi \tag{13}$$

$$P_\beta = \frac{1}{2\pi}\frac{m_{12}(\theta)}{m_{11}(\theta)}\frac{[Q_0 \sin(2\beta)+U_0(1-\cos(2\beta))]}{2I_0} + \frac{\beta}{2\pi} = \xi \tag{14}$$

Generate a random number $P_\xi \in (0,1)$. If $P_\xi > P_\theta$, regenerate the scattering angle θ until $P_\xi \le P_\theta$ is satisfied. Similarly, $P_\xi \le P_\beta$ must be satisfied to define the azimuth angle β.

2.2.2 Calculation of photon free path and updating of scattering information

The distance between two consecutive scattering collisions of a photon is the free path [19]:

$$l = \frac{-ln(rand)}{Kext*C} \tag{15}$$

Where K_{ext} is the extinction coefficient; C is the concentration coefficient [20]; rand is a random number uniformly distributed in the interval (0,1), representing the survival probability of photons in the free path l.

After the photon undergoes scattering, when θ_0 approaches 0° and $|u_z| > 0.9999$, the expression for the direction cosine after scattering is[21]:

$$\begin{cases} u'_x = \sin\alpha\cos\beta \\ u'_y = \sin\alpha\sin\beta \\ u'_z = SIGN(u_z)\cos\alpha \end{cases} \tag{16}$$

Where $SIGN(u_z)$ is the sign function. When $u_z \geq 0$, $SIGN(u_z) = 1$, and when $u_z < 0$, $SIGN(u_z) = -1$. When $|u_z| < 0.9999$, the cosine expression for the scattering direction is:

$$\begin{cases} u'_x = \frac{\sin\alpha(u_x u_z \cos\beta - u_y \sin\beta)}{\sqrt{1-u_z^2}} + u_x \cos\alpha \\ u'_y = \frac{\sin\alpha(u_y u_z \cos\beta + u_x \sin\beta)}{\sqrt{1-u_z^2}} + u_y \cos\alpha \\ u'_z = -\sin\alpha\cos\beta\sqrt{1-u_z^2} + u_z\cos\alpha \end{cases} \tag{17}$$

The position of the photon after scattering is:

$$\begin{cases} x' = x + l * u'_x \\ y' = y + l * u'_y \\ z' = z + l * u'_z \end{cases} \tag{18}$$

When a photon propagates in a medium, after multiple scatterings, the relationship between the outgoing stokes vector S' and the incident stokes vector S_0 is as follows[22]:

$$S' = \begin{bmatrix} I \\ Q \\ U \\ V \end{bmatrix} = R(\beta_n) * M(\theta_n) * R(-\gamma_n) * \cdots * R(\beta_1) * M(\theta_1) * R(-\gamma_1) S_0 \tag{19}$$

Where n is the number of scattering events of the photon in the medium; S_0 is the incident light stokes vector [1;0;0;1]; S′ is the outgoing stokes vector; I is the total light intensity; Q is the intensity difference between the horizontal and vertical directions; U is the intensity difference between the 45° and 135° directions; and V is the intensity difference between the right-hand circularly polarized component and the left-hand circularly polarized component. R(β) is the rotation matrix between the pre-scattering plane and the scattering plane, R(γ) is the rotation matrix between the post-scattering plane and the scattering plane; and M(θ) is the interaction process matrix between the particle and the polarized light.

2.3 Detector reception statistical model

2.3.1 Photon reception judgment

When a photon arrives at the detector plane exactly after the (n+1)th scattering, it is considered a direct arrival, which requires the simultaneous satisfaction of the following two conditions:

1) Axial position attainment conditions

$$z_{n+1} = L \tag{20}$$

Where L is the total transmission distance to the detector.

2) Detector reception criteria

$$x_{n+1}^2 + y_{n+1}^2 \leq (\frac{d}{2})^2 \tag{21}$$

Where d is the detector diameter parameter; x and y are the coordinates of the photon in the detector plane.

When a photon has not yet reached the detector plane in the nth propagation, but has passed through the detector plane in the (n+1)th propagation, it is determined to have crossed and arrived.

1) Axial position attainment conditions

$$z_n < L < z_{n+1} \tag{22}$$

2) The coordinates of the intersection point are calculated as follows:

$$\begin{cases} x = \frac{L-z_n}{z_{n+1}-z_n}(x_{n+1} - x_n) + x_n \\ y = \frac{L-z_n}{z_{n+1}-z_n}(y_{n+1} - y_n) + y_n \end{cases} \tag{23}$$

3) Detector reception criteria

$$x^2 + y^2 \leq (\frac{d}{2})^2 \tag{24}$$

2.3.2 Calculation of polarization degree

Light waves interact with particles such as dust and fog in the atmosphere, resulting in Mie scattering. The light intensity is:

$$I = \frac{\lambda^2}{8\pi^2 r^2} I_0 (i_1 + i_2) \tag{25}$$

Where I_0 and I is the light intensities of the incident light and the outgoing light, respectively; i_1 and i_2 is the scattering intensity functions, expressed as:

$$\begin{cases} i_1 = |S_1|^2 = \left| \sum_{n=1}^{\infty} \frac{2n+1}{n(n+1)} [a_n \pi_n(cos\,\theta) + b_n \tau_n(cos\,\theta)] \right|^2 \\ i_2 = |S_2|^2 = \left| \sum_{n=1}^{\infty} \frac{2n+1}{n(n+1)} [a_n \tau_n(cos\,\theta) + b_n \pi_n(cos\,\theta)] \right| \end{cases} \tag{26}$$

Where S_1 and S_2 are scattering amplitude functions composed of Bessel function and Legendre function; a_n and b_n are scattering coefficients, which are related to the complex refractive index of the particle and the size parameter x=2πr/λ, where λ is wavelength and r is particle radius; π_n and τ_n are functions of scattering angle θ[23].

The intensity $I_\perp$ of the vertically polarized component in the scattered light is expressed as:

$$I_\perp = \frac{\lambda^2}{8\pi^2 r^2} I_0 i_1 \tag{27}$$

The intensity $I_\parallel$ of the parallel polarization component in the scattered light is expressed as:

$$I_\parallel = \frac{\lambda^2}{8\pi^2 r^2} I_0 i_2 \tag{28}$$

In order to study the multiple scattering polarization transmission characteristics of pulsed laser in scattering medium, the pulsed laser beam was discretized into a large number of photons, and the effective photons that reached the detector plane after multiple scattering and were within the time gate were selected, and their stokes vectors were statistically summed [24]:

$$S = \begin{bmatrix} I \\ Q \\ U \\ V \end{bmatrix} = \begin{bmatrix} \sum_{i=0}^{n} I_i \\ \sum_{i=0}^{n} Q_i \\ \sum_{i=0}^{n} U_i \\ \sum_{i=0}^{n} V_i \end{bmatrix} \tag{29}$$

The DOP is expressed as:

$$Dop = \frac{\sqrt{(Q^2+U^2+V^2)}}{I} \tag{30}$$

3 Calculation results and analysis

Using Monte Carlo simulations and extensive photon sampling statistics, the effects of laser pulse width, particle concentration, transmission distance, and particle radius on polarization were studied and analyzed. The incident light wavelength was set to 1064 nm, the laser divergence angle to 1.5 mrad, and the photon number to 10^6. The research subjects were four typical aerosol particles in near-Earth space: water mist particles, biological particles, sea salt particles, and mineral dust particles. The relevant optical parameters of the four typical aerosol particles are shown in Table .1.

Table .1. Key optical parameters for typical aerosol particle types

Aerosol Type	Main Composition	Typical Radius Range (μm)	Complex Refractive Index

Water mist particles	H_2O	1-20	1.33+0i
Bioparticles	Bacteria/Pollen/Spores	0.5-100	1.45 +0.01i
Sea salt particles	$NaCl+H_2O$	0.1-10	1.5 +0.001i
Mineral dust particles	SiO_2/Al_2O_3, etc.	0.1-50	1.55 +0.02i

3.1 Effect of pulse width on polarization degree

Figure. 4 shows the variation of DOP with laser pulse width when circularly polarized light propagates in four typical aerosols with a concentration coefficient of 5, a particle radius of 2 μm, and a transmission distance of 500 m.

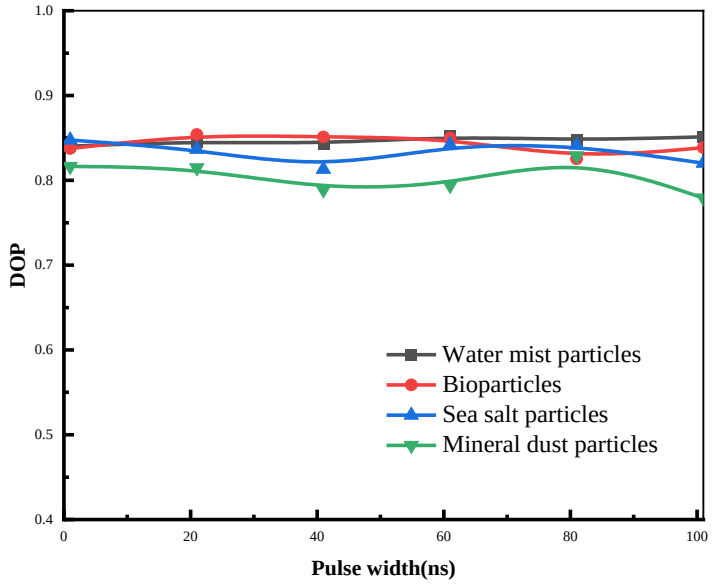

Figure. 4. Polarization characteristics of typical aerosol particles versus pulse width.

As shown in Figure. 4, the DOP in the four typical aerosol particle environments did not change significantly with increasing pulse width. However, significant differences in DOP were observed among different particle types, the highest DOP was observed in the water mist particle environment, followed by the biological and sea salt particle environments, while the lowest DOP was observed in the mineral dust particle environment. Analysis revealed that the reason pulse width variation did not significantly alter the DOP was that, under the same power conditions, narrow pulses corresponded to higher instantaneous photon number densities, while wide pulses corresponded to lower photon number densities. Although the number of incident photons per unit time differed, the probability of photons scattering and colliding with particles was statistically consistent; therefore, the pulse width itself had no significant impact on the polarization state during transmission. Secondly, the difference in the degree of polarization (DOP) among different particle environments mainly depends on the magnitude of the real part of the refractive index. The real part of the refractive index directly affected the intensity of the particle-light interaction, thus determining the asymmetry of the scattering phase function, ultimately manifesting as the difference in polarization characteristics described by the Mueller matrix. The larger

the real part of the refractive index, the stronger the particle's ability to change the polarization state of the incident light in a single scattering event. Under the conditions of fixed particle concentration, particle size and transmission distance, mineral dust particles has the largest real part of refractive index, thus exhibiting the strongest depolarization ability and resulting in the lowest macroscopic DOP. Conversely, water mist particles have the smallest real part of refractive index, and the change in polarization direction by a single scattering is weak, which allows the polarization information to be more effectively maintained in the process of multiple scattering, thus resulting in the highest observed DOP.

3.2 Effect of concentration on polarization degree

Figure. 5 shows the variation of DOP with concentration coefficient when polarized light propagates in four typical aerosols with a pulse width of 10 ns, a particle radius of 2 μm, and a transmission distance of 500 m.

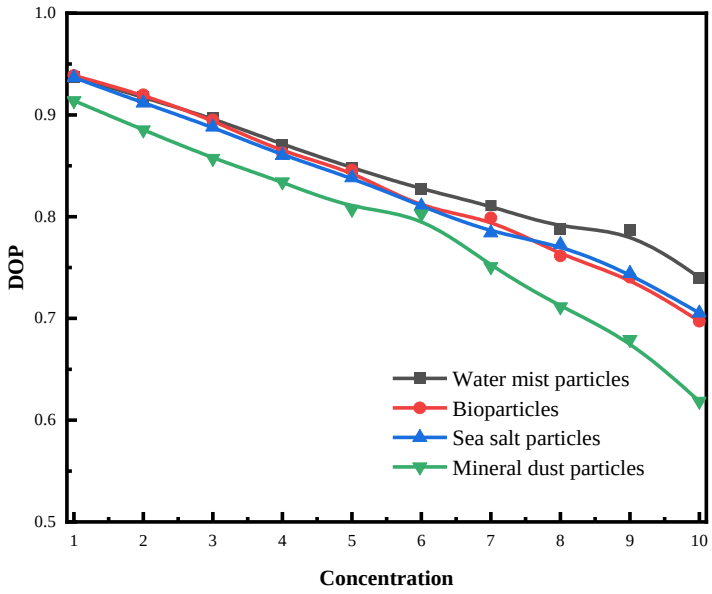

Figure. 5. Polarization characteristics of typical aerosol particles at different concentrations:

As shown in Figure. 5, the DOP of the four typical aerosol particles all decreases with increasing medium concentration. Similar to the effect of pulse width on DOP, the rate of DOP decay varies significantly in different particle environments. The DOP decay is slowest in the water mist particle environment, followed by the biological particle and sea salt particle environments, while the DOP decay is most rapid in the mineral dust particle environment. Analysis reveals that when photons interact with the medium and scatter, their scattering direction is determined by the scattering angle, which in turn affects the scattering phase function of the perpendicular and parallel polarization components. This function directly determines the scattering intensity distribution of different polarization components, leading to significant differences in the intensity of the two components, thus producing a polarization effect. As the medium concentration increases, the mean free path of photons shortens, and the number of scattering events within the same transmission distance increases significantly. Each scattering event may change the polarization state of the photon, and the cumulative effect of multiple scattering processes leads to a decrease in DOP. Furthermore, the real part of the particle's refractive index is a key factor determining the depolarization efficiency of a single scattering event. Mineral dust particles have

the largest real part of the refractive index, resulting in the strongest interaction with light. A single scattering event causes the most significant change in polarization state, leading to rapid destruction of the initial polarization state during multiple scattering events, thus resulting in the fastest DOP decay. In contrast, water mist particles have the smallest real part of the refractive index, and multiple scattering events cause a weaker change in polarization direction. They are better able to maintain polarization information during multiple scattering events, hence their DOP decay is the slowest.

3.3 Effect of transmission distance on polarization degree

Figure. 6 shows the variation of DOP with transmission distance when polarized light propagates in four typical aerosols with a pulse width of 10 ns, a concentration coefficient of 5, and a particle radius of 2 μm.

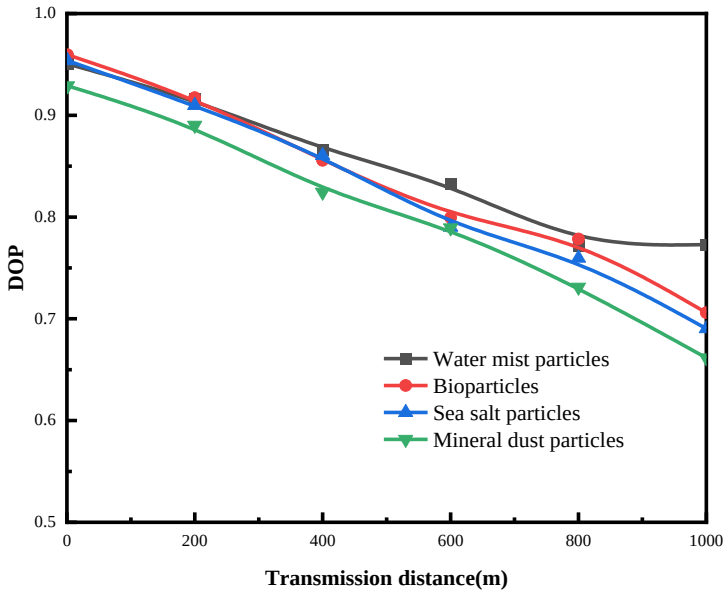

Figure. 6. Polarization characteristics of typical aerosol particles as a function of transmission distance:

As shown in Figure. 6, the DOP in all four typical aerosol particle environments exhibits a monotonically decreasing trend with increasing transmission distance. Among them, the depolarization effect is most significant in the mineral dust particle environment, with the fastest rate of DOP attenuation; the decrease in DOP is slowest in the water mist particle environment; the attenuation rates in the biological particle and sea salt particle environments fall between the two, a trend consistent with the influence of concentration on DOP. Analysis reveals that the increase in the photon propagation path directly leads to a significant increase in the probability of photons encountering scattering events, resulting in more depolarization. Secondly, mineral dust particles have the largest real part of refractive index, exhibiting the highest depolarization efficiency through multiple scattering and the most significant attenuation of DOP. In contrast, water mist particles have the smallest real part of refractive index, thus showing the slowest attenuation trend.

3.4 Effect of particle radius on polarization degree

Figure. 7 shows the variation of DOP with particle radius when polarized light propagates in four typical aerosols with a pulse width of 10 ns, a concentration coefficient of 5, and a transmission distance of 500 m.

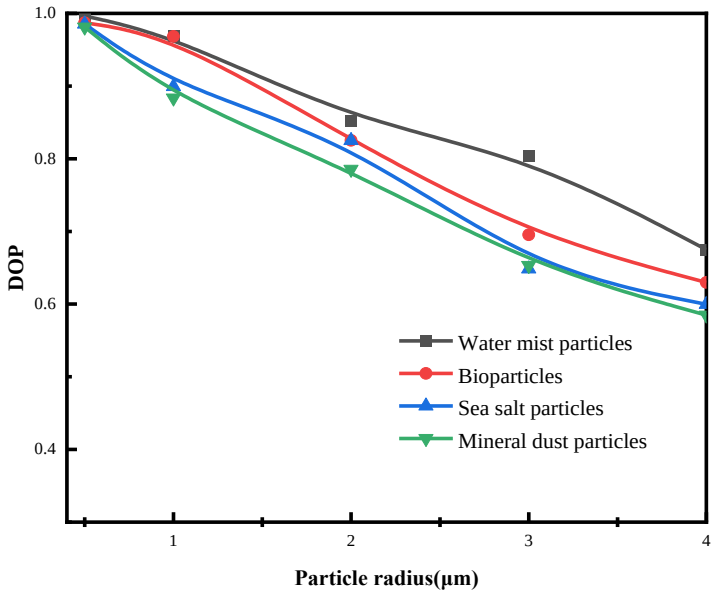

Figure. 7. Polarization characteristics of typical aerosol particles as a function of particle radius.

As shown in Figure. 7, the DOP in all four typical aerosol environments decreases with increasing particle radius, exhibiting a decay rate consistent with the effects of concentration and transmission distance. Specifically, the DOP decreases most slowly in the water mist environment, followed by the biological particle and sea salt particle environments, while the decay is most rapid in the mineral dust environment. Analysis reveals that the increase in particle radius leads to a significant increase in the size parameter x, enhancing interference and phase delay effects within the particles, thus exacerbating the asymmetry of the scattering phase function. This change is directly reflected in the enhancement of depolarization elements in the Mueller matrix, resulting in a stronger ability of a single scattering event to disrupt the polarization state. Secondly, under the condition of constant particle concentration, the increase in radius leads to an increase in the scattering cross section, resulting in an increase in the total scattering coefficient of the medium and a shortening of the photon mean free path, thereby significantly increasing the number of scattering events within the same transmission distance, leading to more depolarization.

3.5 Fitting Model

Based on simulation data, an exponential decay model of DOP with respect to particle properties and transmission parameters was established using the nonlinear least squares method. Fitting results show that this model can effectively characterize the evolution of DOP with respect to particle concentration, radius, transmission distance, and refractive index, with a fitting determination coefficient R^2 of 0.952. This confirms the model's ability to effectively reflect the combined effects of multiple parameters, providing a theoretical basis for the design and parameter optimization of related optical systems.

3.5.1 Model building

By fitting simulation data with refractive indices ranging from 1.3 to 1.6, a functional relationship f(n) of the extinction efficiency factor with respect to the refractive index n was constructed. Based on

this, and combining physical mechanisms and simulation analysis, the following attenuation model for DOP is proposed:

$$P = P_0 * a * exp\,(-b * f(n) * C * r^2 * L) \quad (31)$$

Where P_0 and P are the DOP of the incident and emitted light, respectively, and a and b are undetermined coefficients whose specific values are affected by environmental factors. The model shows that the DOP decreases exponentially with the product of the extinction efficiency factor f(n), particle concentration C, particle radius squared r^2, and transmission distance L. Based on the simulation environment conditions described in this paper, the Levenberg-Marquardt algorithm in Origin software was used for parameter fitting, with a convergence criterion set to 10^{-9}. The fitting results of the model parameters after iterative calculations are shown in Table .2.

Table .2. Model parameter fitting results

Parameter	Fitted Values
a	0.968
b	2.319×10^6
R^2	0.952

3.5.2 Model Validation

To verify the accuracy of the established polarization transmission model, the simulation data and fitting results were systematically compared and analyzed. Figure.8 compares the fitting curves and simulation results of the DOP as a function of concentration in four typical aerosols under the conditions of pulse width of 10 ns, transmission distance of 500 m and particle radius of 2 μm (the red box "■" in the figure is the simulated sampling value (SSV), and the solid line "-" is the fitted value (FV)).

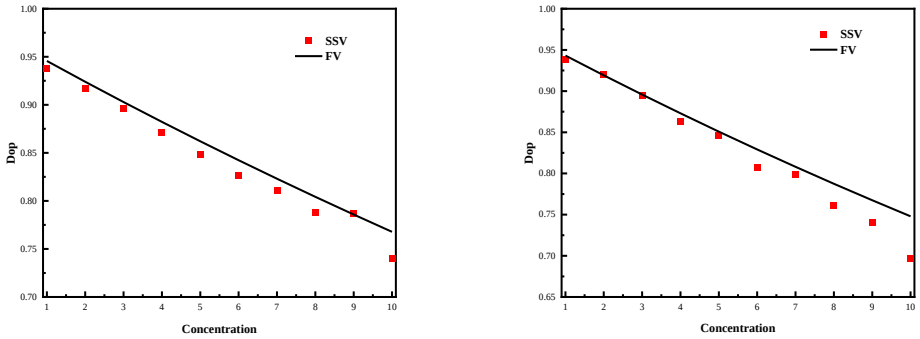

(a) Water mist particles

(b) Bioparticles

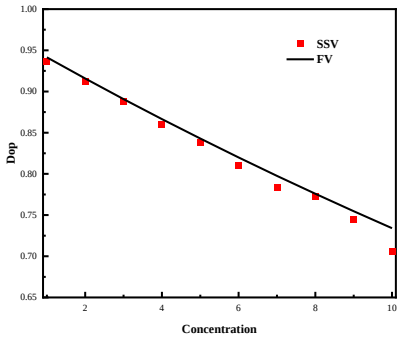

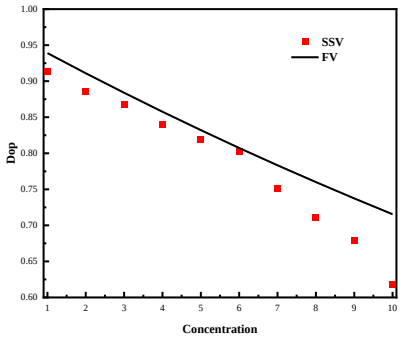

(c) Sea salt particles

(d) Mineral dust particles

Figure.8. Comparison chart of simulation curves and fitting curves for the polarization characteristics of typical aerosol particles at different concentrations.

Figure.8 shows a comparison between the fitted curve of DOP as a function of particle concentration and the simulation results. It can be seen that with the increase of concentration, the DOP in all particle environments shows an exponential decreasing trend. The fitted curve is in high agreement with the simulation data, verifying the model's accurate description of the concentration dependence.

Figure.9 compares the fitting curves and simulation results of DOP as a function of transmission distance in four typical aerosols under the conditions of pulse width of 10 ns, concentration coefficient of 5, and particle radius of 2 μm.

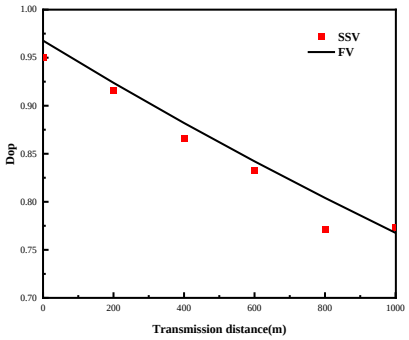

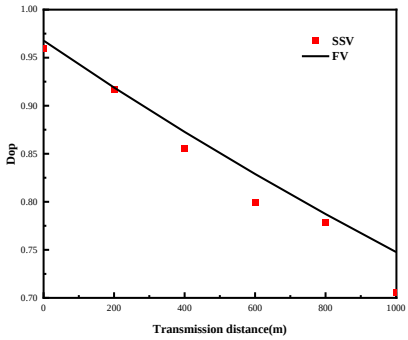

(a) Water mist particles

(b) Bioparticles

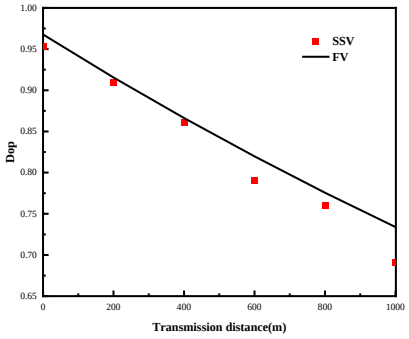

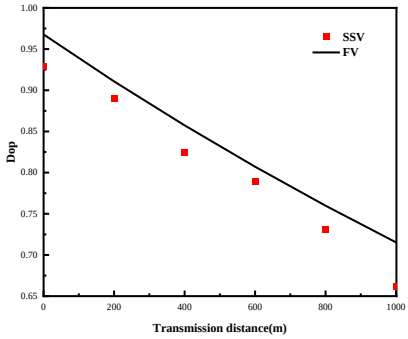

(c) Sea salt particles

(d) Mineral dust particles

Figure.9. Comparison diagram of simulation curves and fitting curves for the polarization characteristics of typical aerosol particles at different transmission distances.

Figure.9 shows the relationship between DOP and transmission distance. With increasing transmission distance, the DOP in all particle environments exhibits an exponential decay characteristic. The consistency between the fitted curve and the simulation data indicates that the model can effectively describe the attenuation behavior of DOP during medium transmission.

Figure.10 compares the fitting curves and simulation results of the DOP as a function of radius in four typical aerosols under the conditions of pulse width of 10 ns, concentration coefficient of 5, and transmission distance of 500 m.

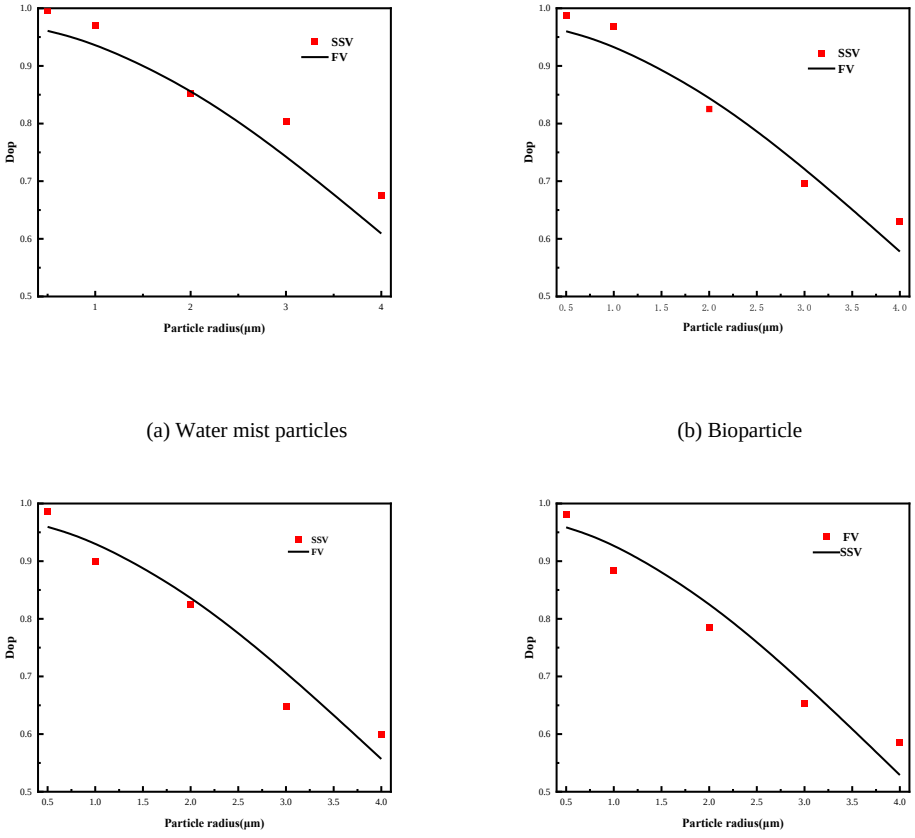

(a) Water mist particles (b) Bioparticle

(c) Sea salt particles (d) Mineral dust particles

Figure.10. Comparison diagram of simulation curves and fitting curves for the polarization characteristics of typical aerosol particles with different radius.

Figure.10 shows the variation of DOP with particle radius. As particle radius increases, the DOP exhibits an exponential decay characteristic in all particle environments. Notably, the radius appears as a square r^2 in the model, reflecting the square relationship between the extinction coefficient and the particle geometry. The fitting results agree well with the simulation data, demonstrating the model's effectiveness in representing particle size effects.

4 Conclusion

This paper addresses the polarization propagation problem of 1064 nm NPCPL in near-surface aerosol environments. Based on Mie scattering theory and the Monte Carlo method, a multiple scattering polarization propagation model was established to simulate the scattering characteristics of four typical

near-surface aerosol particles—water mist, biological particles, sea salt, and mineral dust particles—under different pulse widths, concentrations, transmission distances, and radii. The variation law of DOP was analyzed, and an exponential decay fitting model of DOP with particle concentration, radius, and transmission distance was established based on simulation data. The results show that the DOP attenuation rate varies significantly in different types of particle environments. The DOP attenuation is slowest in water mist particle environment, followed by biological particle and sea salt particle environment, and fastest in mineral dust particle environment. This phenomenon mainly stems from the difference in the real part of the particle refractive index. The larger the real part of the refractive index, the stronger the interaction between the particle and light, leading to a more significant depolarization effect in the single scattering process. Pulse width has a relatively small impact on DOP. Under the same power conditions, although narrow pulses correspond to higher instantaneous photon number densities, the probability of photons colliding with particles is statistically consistent; therefore, changes in pulse width do not significantly affect the polarization state. Both increased medium concentration and transmission distance lead to a decrease in DOP. These factors, by shortening the photon mean free path and increasing the number of scattering events, enhance the cumulative depolarization effect of multiple scattering. The particle radius has the most significant impact on DOP attenuation. This arises from the fact that an increase in particle radius enhances the asymmetry of the scattering phase function, thereby strengthening the depolarizing elements in the Mueller matrix and increasing the ability of a single scattering event to degrade the polarization state. Furthermore, increased radius leads to an increased extinction coefficient, resulting in a higher probability of scattering and thus exacerbating depolarization. Based on the coupled effects of these factors on DOP, this paper further proposes an exponential decay fitting model for DOP, achieving a goodness of fit of 0.952. This model comprehensively reflects the influence mechanism of parameters such as particle concentration, radius, transmission distance, and refractive index on the DOP of polarized light scattering transmitted in the atmosphere.

The proposed typical multi-particle aerosol coupled scattering polarization model can further improve the mechanism analysis of the impact of target polarization detection and provide a theoretical basis for the anti-interference design of systems such as lidar and wireless communication.

Data availability

All relevant data are within the paper

Declaration of competing interest

The authors declare no conflicts of interest.

Acknowledgments

The authors acknowledge the financial support provided within the Natural Science Foundation of Jilin Province, P.R. China, under Project No. 20220101034JC.

References

[1] Kopilevich, Yurij I, Coherent light backscattering by refractive turbulence in the atmospher, Proc. SPIE,2312, 130-135 (1994)

[2] P. Rairoux, H. Schillinger, S. Niedermeier, M.Rodrigue and F. Ronneberger, “Remote sensing of the atmosphere using ultrashort laser pulses”, Appl. Phy. B, 71, 573 – 580 (2000)

[3] HUANG Baoli, HAN Xingwei, ZHANG N an, et al. Pointing deviation correction of satellite laser ranging system [J]. Laser & Infrared, 2014, 44(7): 71 5-719.

[4] ZHAO Xue, ZHANG Xunfang, TANG Rufeng, et al. Research on image p rocessing methods for laser ranging collected by CMOS cameras [J]. Astronomical R esearch & Technology,2018,15(4): 404-412.

[5] Jeffrey O. Coleman. Architecture for a Demonstration Radar-Communication Link[R]. NRL Report 8829. Washington, D.C.: Naval Research Laboratory, 1984:8.

[6] Cochenour, Brandon & Mullen, Linda & Muth, John. (2012). A modulated pulse laser for underwater detection, ranging, imaging, and communications. Proceedings of SPIE - The International Society for Optical Engineering. 8372. 24-.

[7] Poulton C V, Byrd M J, Russo P, et al. Long-range LiDAR and free-space data communication with high-performance optical phased arrays[J]. IEEE Journal of Selected Topics in Quantum Electronics, 2019, 25(5): 1-8.

[8] HU Xiaowei, ZHU Qingsheng, SHA Xiaoming, et al. Research on light sp ot image p rocessing methods for satellite laser ranging [J]. Laser & Infrared, 2020, 50(3): 380-384.

[9] Tang S,Dong Y,Zhang X.Impulse response modeling for underwater wireless optical Communication links[J].IEEE Transactions on Communications,2014,62(1):226-234.

[10] Mishchenko M I, Dlugach J M. Multiple scattering of polarized light by particles in an absorbing medium[J]. Applied optics, 2019, 58(18): 4871-4877.

[11] Meland B, Kleiber P D, Grassian V H, et al. Visible light scattering study at 470, 550, and 660 nm of components of mineral dust aerosol: Hematite and goethite[J]. Journal of Quantitative Spectroscopy and Radiative Transfer, 2011, 112(6): 1108-1118.

[12] Van der Laan J D, Scrymgeour D A, Kemme S A, et al. Detection range enhancement using circularly polarized light in scattering environments for infrared wavelengths[J]. Applied Optics, 2015, 54(9): 2266-74.11111.

[13] Linder, Tomas & Lofqvist, Torbjorn. (2011). Monte Carlo simulation of photon transport in a randomly oriented sphere-cylinder scattering medium. Applied Physics B. 105. 659-664.

[14] Roy G, Tremblay G, Cao X. Scattering phase function depolarization parameter model and its application to water droplets sizing using off-axis lidar measurements at multiple angles[J]. Applied optics, 2018, 57(4): 969-977.

[15] E. B. Shybanov and V. I. Haltrin, "Scattering of light by hydrosol particles suspended in coastal waters," OCEANS '02 MTS/IEEE, Biloxi, MI, USA, 2002, pp. 2374-2382 vol.4.

[16] Wang F, Chen H, Ma C, et al. Construction of backscattering echo caused by cloud in laser fuze[J].Optik,2018,171:1 53-160.

[17] Yun T, Zeng N, Li W, Li D, Jiang X, Ma H. Monte Carlo simulation of polarized photon scattering in anisotropic media. Opt Express. 2009 Sep 14;17(19):16590-602.

[18] Sebastian Bartel and Andreas H. Hielscher, "Monte Carlo simulations of the diffuse backscattering Mueller matrix for highly scattering media," Appl. Opt. 39, 1580-1588 (2000)

[19] Jessica C. Ramella-Roman, Scott A. Prahl, and Steve L. Jacques, "Three Monte Carlo programs of polarized light transport into scattering media: part I," Opt. Express 13, 4420-4438 (2005)

[20] Xu J Y , Gao J , Zhang Y Y ,et al.A study on polarization properties for light scattering and transmission in different-concentration media[J].Tien Tzu Hsueh Pao/Acta Electronica Sinica, 2015, 43(8):1604-1609.

[21] Witt, Adolf. (1977). Multiple scattering in reflection nebulae. I. A Monte Carlo approach. The Astrophysical Journal Supplement Series. 35. 1-6.

[22] Ramella-Roman J C, Prahl S A, Jacques S L. Three Monte Carlo programs of polarized light transport into scattering media: part I[J]. Optics Express, 2005, 13(12): 4420-4438.

[23] He G S , Qin H Y , Zheng Q .Rayleigh, Mie, and Tyndall scatterings of polystyrene microspheres in water: Wavelength, size, and angle dependences[J].Journal of Applied Physics, 2009, 105(1):023110-023110-10.

[24] Zhang Q, Gao J, Xu X, et al. Analysis of multiple scattering polarization transmission properties[J]. Zhongguo Jiguang(Chinese Journal of Lasers), 2012, 39(12): 1213001-8.